Dynamic analysis of soft hang-off riser in deep water, coupling the vibration of lateral and longitudinal directions

Liangjie Mao[1], Song Zeng[1], Qingyou Liu[1*]

[1]State Key Laboratory of Oil and Gas Reservoir Geology and Exploitation, Southwest Petroleum University, Sichuan, Chengdu, 610500, China;

Correspondence author: Qingyou Liu; E-mail: liuqy66@aliyun.com.

Abstract: A dynamic analysis model of soft hang-off riser in deep water is established to analyze the mechanical behavior of a drilling riser. In this model, the riser is suspended by the tensioner at one end and free at the other end. The movement of the riser can be considered as a process coupling the vibration of lateral and longitudinal directions. The model is solved via finite element method (FEM) and verified by the results of ABAQUS and a similar experiment. The riser deformation, bending moment and longitudinal vibration in a well from the South China Sea are analyzed and the influences of the lower marine riser package (LMRP) weight, evacuation and current velocities, desired track of the drilling platform, and the length of the hang-off drilling riser on drilling riser deformation are discussed. The results are of significant importance for the practical operation of soft hang-off drilling riser during evacuation.

Keywords: Drilling riser; deep water; soft hang-off; dynamic analysis

1. Introduction

Drilling risers, which are the connecting channels for the drilling platform and subsea blowout preventer (BOP) system, play an important role in deepwater drilling. However, drilling risers may be easily fractured due to ocean environment load. During an approaching typhoon, the drilling riser

with LMRP may be disconnected from the BOP, whereas the drilling platform with a suspended drilling riser must be evacuated to avoid the typhoon.

The force of drilling risers is highly complex under soft hang-off conditions. The ocean environment may affect the drilling risers. The platform movement may also influence the drilling risers and cause force from seawater. The included angle between the desired track and load direction induced by the ocean environment may considerably influence the force of the drilling risers. Drilling risers may be destroyed when the bending moment surpasses the material strength in theory, thereby triggering accidents and enormous economic losses. Moreover, numerous accidents are caused by the fracture of drilling risers during evacuation in the South China Sea [1].

Several researchers have focused on the mechanical analysis of drilling risers. Mao [2] established a deepwater mechanical behavior analysis model of drilling risers, considering an actual riser string configuration. Fan [3] established a hang-off riser model to analyze the influence of internal solitary wave on riser. The results show that attention should be paid to the impact of LMRP on other equipment on the seabed. Steddum[4] discussed the response of a disconnected riser hanging on a drifting vessel, with particular emphasis on the response of the shear loads to the vessel. Sheng[5] summarized the related experience of CNOOC on responding to severe weather in a hang-off mode and indicated that a contingency plan for a hang-off riser to resist severe weather is feasible. Wu[6] proposed a dynamical model in investigating the dynamic response of the hard hang-off of a riser to evacuate with HYSY 981 drilling platform. A model for a hang-off riser was established to calculate the operation envelope of the hang-off riser during a severe weather [7]. Wang[8] identified influencing factors with respect to technical and commercial considerations that affect the selection of a hang-off

riser system and established selection criteria for each influencing factor, along with the comparison of relative merits of each type of hang-off riser systems. Ambrose et al.[9] investigated the soft hang-off riser models in ultra-deepwater and discussed the feasibility of soft hang-off method and compared the characteristics of the hang-off riser. by analyzing a deep-water drilling riser during installation, Long et al.[10] found that the response of riser increased with the axial storm. Dai[11] presented the effective tension of a drilling riser under operability and hang-off conditions. Yasukawa[12] studied the limiting wave height of a deep-water hang-off riser and discussed the influences of internal fluid mass on the riser and the associated fluid friction on the limiting wave height. Burgdorf[13] evaluated the axial and lateral modal superpositions for a 3D riser, showing that the dominant design parameter that affects the peak loads of hang-off riser is in close to resonance. A mechanical analysis model of deepwater by ABAQUS was established for the deep-water riser considering grounding risk; it demonstrates that the shape of the riser after grounding seabed is catenary [14].

Despite these studies, dynamic mechanical behavior analysis model for drilling risers under soft hang-off conditions, coupling the vibration of lateral and longitudinal directions, is rare. The present study is aimed at investigating the dynamic mechanical behavior of riser under soft hang-off conditions. A dynamic model for a riser under soft hang-off conditions is established and the dynamic model is solved via FEM. Then the model is verified by the results of ABAQUS and an experiment. The influences of the LMRP weight, evacuation and current velocities, desired track of the drilling platform, and the length of the hang-off drilling riser on drilling riser deformation are analyzed. This dynamic analysis model focuses on riser strength and the deformation of riser is large, whereas vortex-induced vibration (VIV) lay emphasis on riser fatigue. So that VIV is not included in

this study.

2. Analysis model

Drilling risers generally adapt a soft hang-off mode given the deep water and enormous wave loads in South China Sea [15]. Under soft hang-off mode, the drilling riser with the LMRP disconnects from the BOP, and the drilling riser is suspended by the tensioner. The tensioner and telescopic joint bear the weight of the drilling riser. The schematic for the soft hang-off riser mode is shown in Fig. 1. The desired track of the drilling platform may be different from the direction of the ocean environment. The riser could be pass as a beam hinged at one end and free at the other and the schematic of the evacuation for a platform is shown in Fig. 2. The movement of the riser can be regarded as a process, coupling the vibration of lateral and longitudinal directions.

2.1 Basic assumptions

In this analysis model, the thickness of the riser is constant along the *z*-axis, and the material is presumed homogeneous and isotropic. The variation of string configuration along the longitudinal direction is ignored. After the riser disconnected from the BOPs, the internal fluid and the external seawater were connected to each other. Thus, the effect of the internal fluid is not considered in the analysis model [2, 5, 7]. Because the displacement is much larger than the diameter of the riser during evacuation, the damping on the riser is neglected. The length of the riser is considerably larger than its diameter. Hence, the riser is an entity of slender cylinder beam, and the bending on the joint that contacts two single risers is neglected [16].

2.2 Riser model and governing equation

The drilling riser is a beam with hinges at the upper ends; thus, the movement of riser could be described by the governing equation of vibration of the suspension beam in terms of material strength. The entire riser is divided into infinitesimal element. The movement of each element subjected to forces from the *x*- and *z*-axes can be described by lateral velocity *u*, longitudinal velocity υ, and deflection θ. The schematic of forces and movement is shown in Fig. 3. Thus, according to Hamilton theory, by coupling the lateral and longitudinal movements, the differential governing equation for the riser can be represented as follows [17]:

$$\begin{cases} \rho A\dfrac{d^2u}{dt^2} - EA\dfrac{\partial^2 u}{\partial z^2} = F_{\mathrm{u}} + \xi EA\dfrac{\partial \upsilon}{\partial z}\cdot\dfrac{\partial^2 \upsilon}{\partial z^2} \\ \rho A\upsilon + EI\dfrac{\partial^4 \upsilon}{\partial z^4} + \rho I\dfrac{\partial^2}{\partial t^2}\left(\dfrac{\partial^2 \upsilon}{\partial z^2}\right) = F_{\upsilon} + EA\left[\xi\left(\dfrac{\partial^2 u}{\partial z^2}\cdot\dfrac{\partial \upsilon}{\partial z} + \dfrac{\partial u}{\partial z}\cdot\dfrac{\partial^2 \upsilon}{\partial z^2}\right) + \dfrac{3}{2}\xi^2\left(\dfrac{\partial \upsilon}{\partial z}\right)^2\dfrac{\partial^2 \upsilon}{\partial z^2}\right] \end{cases}, \quad (1)$$

where ρ denotes the material density (g/cm^3), *A* is the cross-sectional area (m^3), *t* denotes time (s), *u* is the riser axial deflection (m/s), υ is the riser transverse deflection (m/s), and *E* represents Young's modulus (Pa). F_{u} is the axial direction force distribution along the *z*-axis (*N*), ξ denotes the coupling factor that is equal to 1 in the nonlinear system, *I* is the area moment (*N*), and F_{υ} is the lateral force (*N*).

2.3 Boundary conditions

The drilling riser is a beam hinged by the tensioner. Hence, the riser moving with platform along the x-axis direction and the top end of riser would rate in a specific angle, the rotation stiffness of the UFJ is *K*u. The upper boundary conditions can be expressed as follows:

$$\begin{cases} u(0,t) = u_{\text{boat}}(t) \\ \upsilon(0,t) = 0 \\ K_{\text{u}} \dfrac{\partial \upsilon}{\partial z} + EI \dfrac{\partial^2 \upsilon}{\partial z^2} = 0 \end{cases}, \tag{2}$$

where u_{boat} is the speed of the platform (m/s), and K_u is the rotation stiffness of the UFJ ($\text{N}\bullet\text{m}/\text{deg}$).

Meanwhile, the other end of the riser is free from any restraint. However, the bottom of the riser must bear the weight of the LMRP. Thus, the lower boundary conditions can be expressed as follows:

$$\begin{cases} EA\left(\dfrac{\partial u}{\partial z} + \dfrac{\xi}{2}\left(\dfrac{\partial \upsilon}{\partial z}\right)^2\right) + M_{\text{LMRP}} \dfrac{d^2 u}{dt^2} = 0 \\ \dfrac{\partial}{\partial z}\left(EI \dfrac{\partial^2 \upsilon}{\partial z^2}\right) - \rho I \dfrac{\partial}{\partial z}\left(\dfrac{d^2 \upsilon}{dt^2}\right) - EA\left(\xi \dfrac{\partial u}{\partial z} + \dfrac{\xi^2}{2}\left(\dfrac{\partial \upsilon}{\partial z}\right)^2\right)\dfrac{\partial \upsilon}{\partial z} - M_{\text{LMRP}} \dfrac{d^2 \upsilon}{dt^2} = 0, \\ EI \dfrac{\partial^2 \upsilon}{\partial z^2} = 0 \end{cases} \tag{3}$$

where M_{LMRP} is the mass of LMRP (kg).

3. Ocean environment loads

The loads applied to the riser comprise the weight of lower LMRP, the weight of the risers and ocean environment loads. The risers are slender cylinders. Thus, the main ocean environment loads can be simulated by the Morison equation. The cylinder moves with the loads and the displacement of the platform. Therefore, the ocean environmental loads can be calculated as follows [18, 19]:

$$f_{\text{w}} = \frac{1}{2} C_{\text{D}} \rho_{\text{w}} D \left(v_{\text{w}} - \frac{dx}{dt}\right)\left|\left(v_{\text{w}} - \frac{dx}{dt}\right)\right| + C_{\text{M}} \rho_{\text{w}} \frac{\pi D^2}{4} \frac{dv_{\text{w}}}{dt} - C_{\text{m}} \rho_{\text{w}} \frac{\pi D^2}{4} \frac{dv_{\text{w}}}{dt} \frac{d^2 x}{dt^2}, \tag{4}$$

where C_{D} is the drag force coefficient; ρ_{w} is the density of sea water (kg/m^3); D is the outer diameter of the riser (m); v_{w} is the horizontal velocity of the wave water (m/s); x is the

displacement of the riser (m); $\frac{dx}{dt}$ is the horizontal velocity of the riser caused by loads and the boat movement; C_{m} is the added mass coefficient; C_{M} is the inertia force coefficient, which can be calculated by $C_{\mathrm{m}}+1$.

4. Solution of the model

Finite element and Newmark-β methods are used to dissolve the differential governing equation (Equation 1) of the riser. The Lagrange function and Hermite interpolation method indicate that the finite element formula of the longitudinal displacement u and lateral displacement υ can be represented as follows [17, 20]:

$$\begin{cases} u = \boldsymbol{\psi}^T \boldsymbol{d} \\ \upsilon = \boldsymbol{\varphi}^T \boldsymbol{d} \end{cases}, \tag{5}$$

$$\boldsymbol{d} = \left[u_1 \quad \upsilon_1 \quad \frac{d\upsilon_1}{dx} \quad u_2 \quad \upsilon_2 \quad \frac{d\upsilon_2}{dx} \right]^T, \tag{6}$$

$$\boldsymbol{\psi} = \left[1-\frac{x}{l} \quad 0 \quad 0 \quad \frac{x}{l} \quad 0 \quad 0 \right]^T, \tag{7}$$

$$\boldsymbol{\varphi} = \left[0 \quad \boldsymbol{\varphi_1} \quad \boldsymbol{\varphi_2} \quad 0 \quad \boldsymbol{\varphi_3} \quad \boldsymbol{\varphi_4} \right]^T, \tag{8}$$

$$\begin{cases} \boldsymbol{\varphi_1} = 1-\dfrac{3x^2}{l}+\dfrac{2x^3}{l} \\ \boldsymbol{\varphi_2} = x-\dfrac{2x^2}{l}+\dfrac{x^3}{l^2} \\ \boldsymbol{\varphi_3} = \dfrac{3x^2}{l^2}-\dfrac{2x^3}{l^3} \\ \boldsymbol{\varphi_4} = -\dfrac{x^2}{l}+\dfrac{x^3}{l^2} \end{cases}, \tag{9}$$

where l is the length of one element.

The element mass matrix $[M]^e$ can be determined by:

$$[M]^e = \int_0^l \rho A \psi \psi^T dx + \int_0^l \left(\rho A \varphi' \varphi'^T + \rho I \varphi' \varphi'^T \right) dx , \tag{10}$$

The element stiffness matrix can be described as follows:

$$[K]^e = K_1 + K_2 + K_3 + K_3^T + K_4 , \tag{11}$$

$$\begin{cases} K_1 = \int_0^l EA \boldsymbol{\psi}' \boldsymbol{\psi}'^T dx \\ K_2 = \frac{1}{4} \xi^2 \int_0^l EA \boldsymbol{\varphi}' \boldsymbol{\varphi}'^T \upsilon \upsilon^T \boldsymbol{\psi}' \boldsymbol{\psi}'^T dx \\ K_3 = \frac{1}{2} \xi \int_0^l EA \boldsymbol{\varphi}' \boldsymbol{\varphi}'^T \upsilon^T \boldsymbol{\psi}' dx \\ K_4 = \int_0^l EI \boldsymbol{\varphi}'' \boldsymbol{\varphi}''^T dx \end{cases} , \tag{12}$$

The governing equation can be present as follows:

$$[M]\{u''\} + [K]\{u\} = F(t) , \tag{13}$$

where $[M] = T[M]^e$, $[K] = T[K]^e$, $[M]$ is the global mass matrix, $[K]$ is the global stiffness matrix, and T is the transformation matrix for transforming partial coordinate to global coordinate.

Equation (13) could be solved by the Newmark-β method. The detail of the solution process has been introduced in the literature [2].

5. Validity of the analysis model

A scholar simulated a hang-off riser by using ABAQUS software with marine engineering

module ABAQUS/Aqua and presented the distribution of horizontal displacement in 12 s [14]. For a thorough comparison, we adopt the parameter of ABAQUS model to verify our calculation module, and the maximum deformation of the ABAQUS is selected for comparison with our numerical results. As shown in Fig. 4, the result of our analysis model is in good agreement with that of the ABAQUS, which can prove the accuracy of our model.

To verify the practicality of the calculation module, we conduct an experiment in the Southwest Petroleum University. Fig. 5 shows a photograph of the experimental circular cistern. The experimental marine riser is made of PE that can rotate around the center of the circular cistern. The major properties of the riser and the basic parameters of the calculation model are shown in Table 1.

We regard uniform flow, which is generated by the movement of riser, as the ocean current load in this experiment to stimulate the environmental loads. Strain gauges are attached to the surface of the riser to collect the deformation data, as shown in Fig. 6. To guarantee the accuracy of the stimulated result, we can eliminate the influence of VIV on the deformation of the riser using a mean value treatment in the longitudinal direction. Fig. 7 presents the comparison result of deformation between the calculation model and the experiment. The actual shear flow is assumed as a uniform flow, and the upper part of the riser is fixed due to the limit of the water depth in this experiment, thereby resulting in the differences of deformation between the numerical and experimental data. As the experimental parameter is great different from the actual drilling, experiment only can be regard as a reference, and a more veritable experiment may cost great more.

6. Application and case study

6.1 Riser model analysis

The dynamic response characteristics of the riser in a deep-water well in the South China Sea are analyzed, and the main properties [2] of the riser system are given in Table 2. The hydrodynamic properties of the South China Sea [2, 21, 22] are listed in Table 3. The distribution of surface current speed in South China Sea [15] is shown in Fig. 8.

The model is solved through the finite element method, and the riser is divided into 50 elements of equal length. The time step is set as 0.00163 s, and the calculated results vary with time. Moreover, we focus on the major factors of deformation, bending moment, and longitudinal vibration. In this analysis model, the upper section of the riser moves with the platform in a specific speed while the water flows. The disposal of the direction of the two speeds is shown in Fig. 3. Thus, the relative velocity of the platform and surface current is calculated as the ocean environmental load. Then, the position of the platform is set as the origin point of the coordinates in the calculation.

Figure 9a presents the lateral displacement along the axial direction of the riser at 130 s. The lateral displacement increases rapidly with the increase in water depth and the largest displacement reaches 58.2 m at the LMRP site. However, the lateral displacement close to LMRP increases gradually; the riser in this part is vertical. The weight of the LMRP is considerably larger than that of a single riser; thus, a heavier object has a larger inertia, which is the force that keeps an object in the original position until it moves [9].

Figure 9b shows the bending moment along the axial direction of the riser at 130 s. The bending

moment near the UFJ is large, and the maximum bending moment of 52 KN·m is located near the water surface. The bending moments at other positions of the riser are small but unstable due to the movement of the riser is a dynamic process, and the bending moment only reflects the relative degree of deformation in one moment. The surface of water is the boundary of the loads and is where the loads reach a high point [2, 15]. Thus, deformation increases suddenly, the curve of the lateral displacement is rough near the water surface, and the value of the bending moment is large.

Figure 9c shows the changes in the lateral displacement along the axial direction of the riser at 10, 40, 70, 100, and 130 s. The figure vividly presents the dynamic variation progress of the riser with time. At 10 s, as the riser starts to move, the deformation of all risers is small. As time passes by, the deformation increases smoothly, the lower segments of the riser consistently have a larger deformation than that of the upper segments, maximum displacement is constantly located near the LMRP. In our study, the riser is regard as a soft beam restrained on the upper end, which is subjected to the law of the deformation of the suspended beam [17]. Meanwhile, the other end of the riser is free from any restrain, and its deformation is the largest in our model.

Figure 9d shows the longitudinal vibration responses of the riser at locations of 0, 1000, and 1500 m. The frequency of the vibration curve is consistent at all positions. However, the amplitude evidently increases with the water depth. The initial sinusoidal vibration is applied on the platform in our hypothesis; thus, the response of the longitudinal vibration at 0 m is a standard sinusoidal wave. At the depths of 1000 and 1500 m, the floor level of the amplitude increases compared with that of the initial sinusoidal wave. At the incipient stage, the longitudinal deformation of the riser is small. The floor level of the amplitude at this stage is lower than that of the initial sinusoidal wave.

However, at the subsequent stage, the entire response of the riser increases with the loads increases. Stretching the riser causes the level of the curve to clamp gradually.

6.2 Influence of LMRP weight on riser mechanical behavior

Figure 10 presents the distribution of the riser lateral displacement, bending moment, and longitudinal vibration for the deep-water well under the LMRP weight change from 140 t to 120 t. In the hang-off model, LMRP is a massy plummet connected to the lower end of the riser. It moves gradually with the upper riser. Fig. 10a shows that the riser lateral displacement increases from top to bottom of riser and reaches the maximum displacement at the bottom end. The lateral displacement of the riser increases with the increase in LMRP weight from 140 t to 120 t. Thus, the maximum displacement of 62.7 m is reached at the lower end with the LMRP weight of 120 t. Fig. 10b shows that the bending moment of the riser decreases with the increase in LMRP weight. Moreover, the maximum bending moment occurs at the position close to the upper end. The distribution of ocean environmental loads is shown in Fig. 8. The loads applied onto LMRP are considerably smaller than those close to the upper end. The upper section consistently moves faster than the lower part because the movement of the riser is stimulated by the loads and platform movement. Thus, the state of the riser is oblique. The component force of the weight drags the riser to become vertical, and a heavy LMRP causes difficulty for the riser to move. Meanwhile, a heavier LMRP indicates a larger inertia, thereby damping the movement of the riser in deep water [9]. Fig. 10c shows that the longitudinal vibration of the lower end of the riser decreases with the increase in LMRP weight during the entire evacuation process. All four curves have similar sinusoidal wave and trend. However, in detail, the amplitude is large when the LMRP is not heavy. As shown in Fig. 10a, the largest lateral

displacement occurs in 120 t. Thus, LMRP weight is an obstruction to the movement of the riser. Therefore, the riser with the weight of 120 t is clearly stretched, and the extent of the vibration is large. Thus, a heavy LMRP is beneficial to reduce the deformation of the riser and protect the riser in the evacuation process. Therefore, the platform with a heavier LMRP could evacuate in a large velocity to keep the riser safe [23].

6.3 Influence of surface current speed on riser mechanical behavior

Figure 11 shows the distributions of the riser lateral displacement, bending moment, and longitudinal vibration with the surface current speeds of 1.0, 1.1, and 1.2 m/s, respectively. The riser lateral displacement and bending moment decrease with the fluid velocity increase. In this case, the platform velocity is 1.289 m/s, which is larger than the surface current velocity. The relative speed between the water and the platform decreases with the increase in fluid speed, thereby inducing the decrease in environmental loads and the deformation of the riser. Morison's equation [18] implies that the environment is directly proportional to the speed difference between the surface current and the platform. Moreover, as the surface current speed increases, the amplitude of vibration decreases with the increase in lateral displacement. However, the frequency and trend of the curve remain similar. Thus, a small relative speed between the water and the platform is advantageous to reduce the deformation of the riser [5, 6].

6.4 Influence of platform speed on riser mechanical behavior

Figure 12 shows the distribution of the riser lateral displacement, bending moment, and longitudinal vibration with the platform speeds of 2.4, 2.5, and 2.6 knots, respectively. Both of them increase with the fluid speed. In this case, the velocity of surface current is 1.2 m/s, which is smaller

than the smallest platform velocity of 2.4 knots (1.23 m/s). Thus, the relative speed between the water and the platform decreases with increase in surface current speed. Fig. 8 shows the distribution of the environmental loads, which indicating that the entire environmental loads applied to the riser increase with the velocity of surface current, thereby weakening the dynamic vibration process while the weight of the riser is unchanged [5, 6]. Therefore, the change in vibration amplitude with the increase in surface current speed is small, as shown in Fig. 12c. Consequently, maintaining a platform speed close to the surface current is a suitable approach to protect the riser under the evacuation condition.

6.5 Influence of the desired track of drilling platform on riser mechanical behavior

Figure 13 presents the influence of the desired track of the drilling platform on the distributions of riser lateral displacement, bending moment, and longitudinal vibration. The velocity of the surface is larger than that of the platform, and the track disposal of the platform is shown in Fig. 2. As the relative speed between the platform and the surface current decreases, the lateral displacement declines with the angle rises. When the angle is 90°, the relative speed is equal to the platform speed. Therefore, the direction of the deformation is contrary to angles 0° and 45°. When the angle is 0°, the direction of the velocities of the platform and the surface current are the same, and the relative speed reaches a high point. Thus, the deformation and amplitude are considerably larger than the others. Angles larger than 90° are not discussed in this study because they increase the relative speed, which increases the deformation of the riser. Consequently, when the surface current speed is considerably bigger than that of the platform, driving the platform against the surface current direction during evacuation is dangerous [23].

6.6 Influence of suspension length on riser mechanical behavior

Figure 14 shows the influence of suspension length on the distributions of lateral displacement, bending moment, and longitudinal vibration of the riser. The lateral displacement and bending moment of the riser remarkably increase with the length of the riser. Fig. 14c shows that the amplitude of the vibration curve increases with the suspension length. When the riser is short (1200 m), the entire weight and the flexibility of the riser are also small. The movement of the riser directly reflects the stress response of the environmental loads and platform movement. Meanwhile, the environmental load of the surface current is considerably larger in the water surface (Fig. 11). A short riser easily moves due the response of furious surface current loads, whereas a long and heavy riser does not respond because rigid bodies stop the movement but exhibit axial stretch and contraction, thereby magnifying the tension excursions of the riser. The movement of a long riser is an elastic response under the environment and self-weight loads [10]. Therefore, a short riser is beneficial to reduce the deformation of the entire riser but is harmful to the UFJ. Taking back a part of the riser before evacuation could apparently reduce the degree of the deformation [4, 5, 23].

7. Discussion

In the evacuation condition, the soft hang-off mode riser is likely to generate largest deformation due to the rotational stiffness of the top end. Risers may be easily fractured if the deformation and bending moment surpass their maximal limitation. Meanwhile, a large longitudinal vibration may cause grounding accident and damage the LMRP, tensioner, and moon pool. We concluded several operation suggestions during evacuation by analyzing the influences on the dynamical mechanic behavior of soft hang-off the riser.

A heavier LMRP is beneficial to moderate the movement of riser and enhance the available velocity of the platform, but, generally, it is unchangeable in a specific case. Environmental load is greatly affects the deformation of the riser. Different combinations of velocity of surface current, velocity of platform, and the desired track of platform influence the environment mainly by changing the relative velocity between water and platform. Therefore, the velocity of the platform must be maintained at a lower level and the desired track must not be against the direction of the surface current during evacuation to reduce the deformation of the riser and to protect the riser and the upper flex joint (UFJ) [5, 15]. In addition, taking back part of the riser in an appropriate degree is a feasible operation for protecting the riser, because it could not only reduce the weight of the riser and the lateral displacement, but also reduce the longitudinal vibration, which could effectively avoid the grounding accident [4, 5]. However, unceasingly taking back the riser to reduce its suspension length is discouraged because a short suspension riser easily sinks and rises given the direct effect of surface current, thereby damaging the tensioner and telescope joint [23]. Moreover, consuming excessive time on taking back the riser, may cause failure to achieve the best opportunity to evacuate safely.

8. Conclusions

The distribution of riser lateral displacement, bending moment and longitudinal vibration decrease with the increases the weight of LMRP, the variation of lateral displacement with the change of LMRP weight mainly occurs at the parts close to LMRP. The velocity of surface current, velocity of platform and the desired track of platform jointly determine the relative velocity between surface current and platform. A large relative velocity between surface current and platform will significantly increasing the lateral displacement, bending moment and longitudinal vibration of riser.

The length of riser has a obviously effect on riser dynamical behavior, the deformation of riser increases with the increases of riser length. But the variation of riser length will apparently affect the manner of dynamic movement of riser.

Acknowledgments

The authors gratefully acknowledge the financial support of the National Natural Science Foundation of China (No. 51604235), Scientific Research Starting Project of SWPU (No. 2015QHZ007)

References

1. Xu, L., Zhou, J., Wang, R., Jiang, S. and Sheng, L., Analysis of deep water drilling platform evacuation from imminent typhoons with riser hang-off in South China Sea. *China Offshore Oil and Gas.*, 2015, **27**(3), 101-107.
2. Mao, L., Liu, Q., Zhou, S., Wang, G. and Fu, Q., Deep water drilling riser mechanical behavior analysis considering actual riser string configuration. *Journal of Natural Gas Science & Engineering.*, 2016, **33**, 240-254.
3. Fan, H., Li, C., Wang, Z., Xu, L., Wang, Y.and Feng, X., Dynamic analysis of a hang-off drilling riser considering internal solitary wave and vessel motion. *Journal of Natural Gas Science & Engineering*., 2017, **37**, 512-522.
4. Steddum, R., The management of long, suspended strings of tubulars from floating drilling vessels. Offshore Technology Conference, 2003.
5. Sheng, L., Xu, L., Zhou, J., Jiang, S. and Li, X., Experience on deepwater drilling riser about hang-off modes in typhoon condition of South China Sea. Offshore Technology Conference. 2016.

6. Wu, W., Wang, J., Tian, Z., Fu, S., Liu, Z. and Luo, J., Dynamical analysis on drilling riser evacuated in hard hang-off mode. International Ocean and Polar Engineering Conference, Busan, 2014.
7. Liu, X., Chen, G., Chang, Y., Fu, J. and Ji, J., Weak point and operation analysis of deepwater drilling riser system in typhoon condition. International Society of Offshore and Polar Engineers, San Francisco, 2017.
8. Wang, Y., Cao, J., Sha, Y., Duan, M., Wang, D., Dong, Y. and Zhou, Y., SCR hang-off system selection considerations and criteria. International Society of Offshore and Polar Engineers, Hawaii, 2011.
9. Ambrose, B. D., Grealish, F. and Whooley, K., Soft hangoff method for drilling risers in ultra deepwater. Offshore Technology Conference, 2001.
10. Long, J. R., Steddum, R. and Young, R. D., Analysis of a 6,000-ft riser during installation and storm hangoff. Offshore Technology Conference, 1983.
11. Dai, W., Gao, F. and Bai, Y., FEM analysis of deepwater drilling risers under the operability and hang-off working conditions. Journal of Marine Science and Application, 2009, **8**(2), 156-162.
12. Yasukawa, H., Ozaki, M. and Tanabe, A., Tension variation and limiting wave height of a deep sea drilling riser in hang-off mode. *Journal of the Japan Society of Naval Architects & Ocean Engineers*., 2009, **1997**(182), 187-198.
13. Burgdorf, O. Jr., Evaluation of axial and lateral modal superposition for general 3d drilling riser analysis. Offshore Technology Conference, 1996.
14. Liu, X., Chen, G., Chang, Y., Liu, K., Zhang, L. and Xu, L., Analyses and countermeasures of deepwater drilling riser grounding accidents under typhoon conditions. *Petroleum Exploration &*

Development., 2013, **40**(6), 791-795.

15. Qi, J., A Study on structure dynamics and vortex shedding vibration of drilling risers under hang off mode. Shanghai Jiao Tong University, Shanghai, 2015.
16. Wang, J., Duan, M., He, T. and Jing, C., Numerical solutions for nonlinear large deformation behaviour of deepwater steel lazy-wave riser. *Ships & Offshore Structures*., 2014, **9**(6), 655-668.
17. Xing, Y. and Liang, K., Nonlinear vibration analysis of longitudinal-transverse coupled beam. *Journal of Beijing University of Aeronautics & Astronautics*., 2015, **41**(8), 1359-1366.
18. Morison, J. R., The force exerted by surface waves on piles. *Journal of Petroleum Technology*., 1950, **189**(5), 149-154.
19. Han, S. M. and Benaroya, H., Non-linear coupled transverse and axial vibration of a compliant structure, part 1: formulation and free vibration. *Journal of Sound & Vibration*., 2000, **237**(5), 837-873.
20. Liu, J., Zhao, H., Liu, Q., He, Y., Wang, G. and Wang, C., Dynamic behavior of a deepwater hard suspension riser under emergency evacuation conditions. *Ocean Engineering.*, 2018, **150**, 138-151
21. Fang, H.C., Dong, S.P., Jin, F. and Xu, X.P., Experiment and study of the drag coefficient for drilling riser. *Oil Field Equipment*., 1987, **15** (2), 1-6.
22. Wang, S.Q. and Liang, B.C., *Wave mechanics for ocean engineering*. Ocean University of China Press, Qindao, 2013.
23. Brekke, J., Soles, J., Wishahy, M. and Stahl, M., Drilling Riser Management for a DP Drillship in Large, Rapidly - Developing Seastates in Deepwater. Society of Petroleum Engineers, 2004.

Table 1 Main physical properties of the drilling riser model

Item	Value
Model length (m)	0.5
Thickness (m)	0.001
Outer diameter (m)	0.0065
Density (kg/m^3)	950
Young's modulus (GPa)	0.8
Density of the basin water (kg/m^3)	1000

Table 2 Main properties of the riser system

Property	Value	Unit
Outer diameter of riser	0.5334	m
Wet weight of a single bare riser	439	Kg
Density of the riser material	7850	Kg/m^3
Modulus of elasticity	210	GPa
Total length of the riser	1800	m
Density of seawater	1025	Kg/m^3
LMRP mass	140000	Kg
Length of a single riser	23.7	m
Rotational stiffness of the upper flex joint	8800	$N \cdot m / deg$
Platform velocity	1	m/s
Flow velocity	1	m/s

Table 3 Hydrodynamic properties in South China Sea

Property	Value	Unit
Drag coefficient C_D	1.2 (between the water surface and 150 m depth) 0.7 (between 150m and the seabed)	Zero dimension
Inertia coefficient C_m	2.0 (at all depths)	Zero dimension

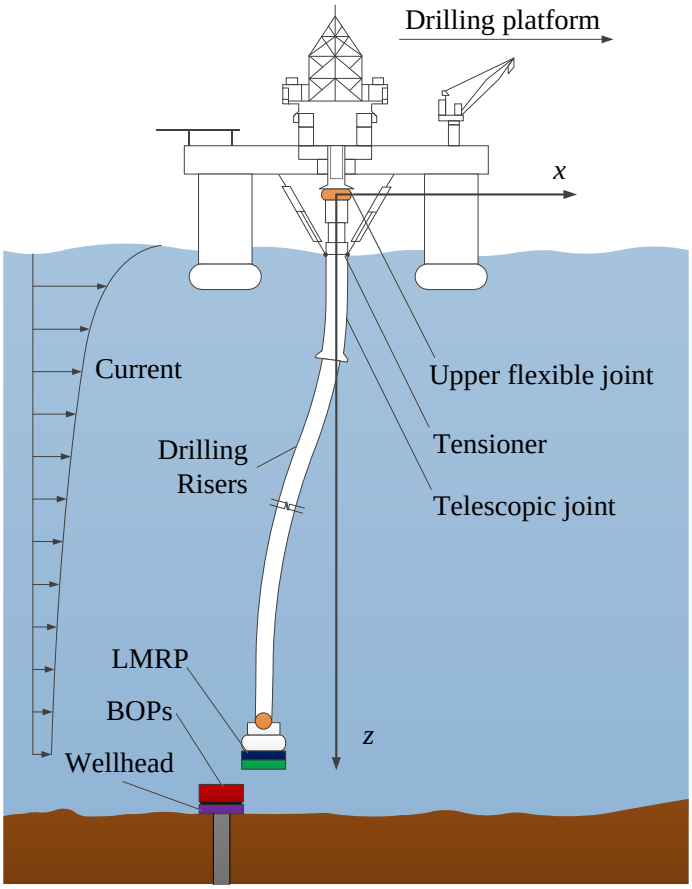

Fig. 1 Schematic for soft hang-off mode of a drilling riser.

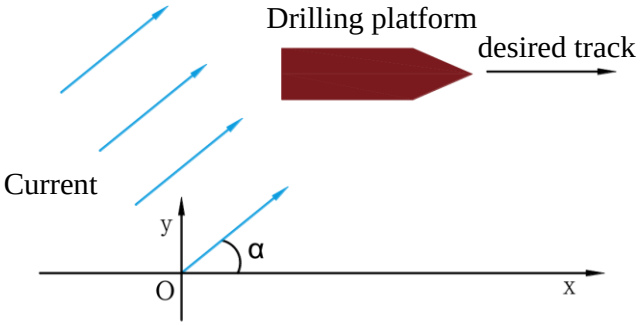

Fig. 2 Schematic of evacuation.

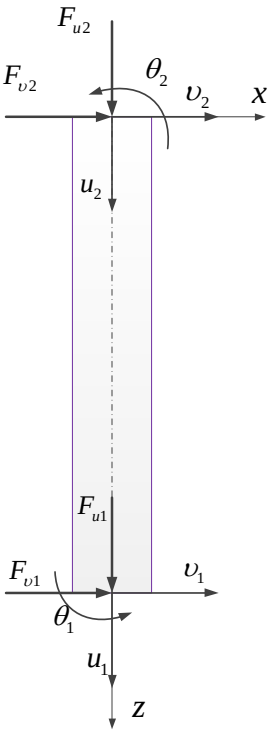

Fig. 3 Schematic of force and displacement.

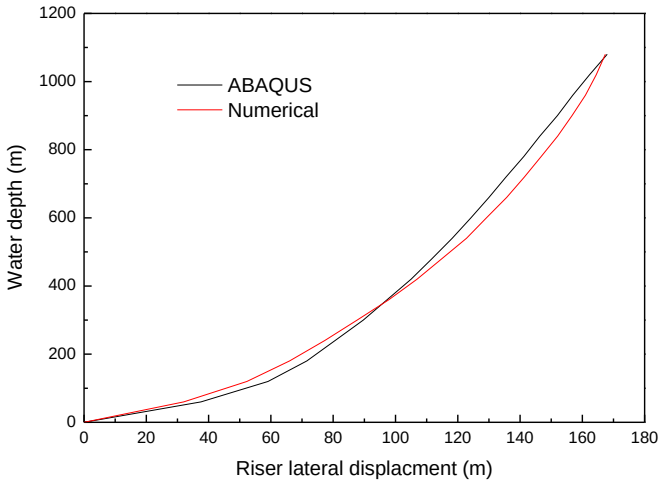

Fig. 4 Comparison of the numerical and ABAQUS results.

Fig. 5 Experimental photograph of the drilling riser.

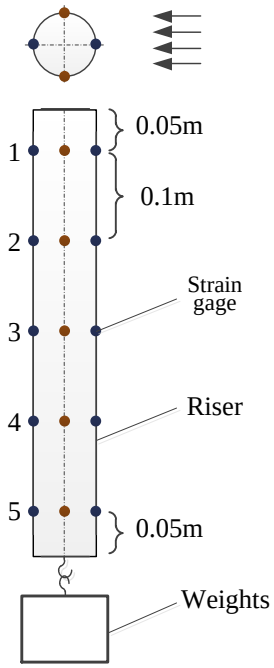

Fig. 6 Arrangement of the strain gauge.

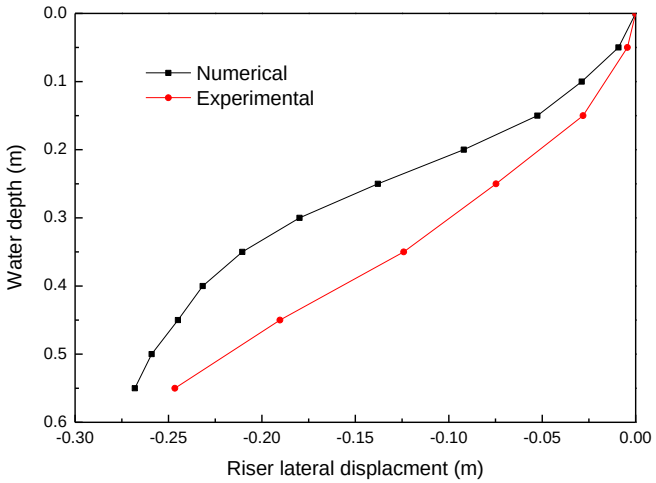

Fig. 7 Comparison of the numerical result and experimental results.

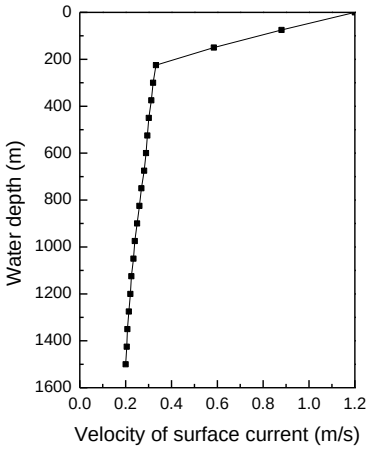

Fig. 8 Distribution of surface current speed.

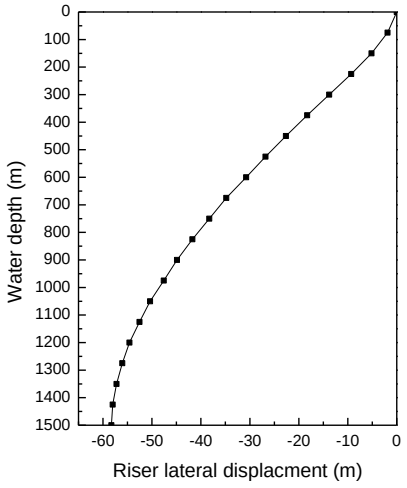
Water depth (m)
0
100
200
300
400
500
600
700
800
900
1000
1100
1200
1300
1400
1500
-60
-50
-40
-30
-20
-10
0
Riser lateral displacment (m)

a)

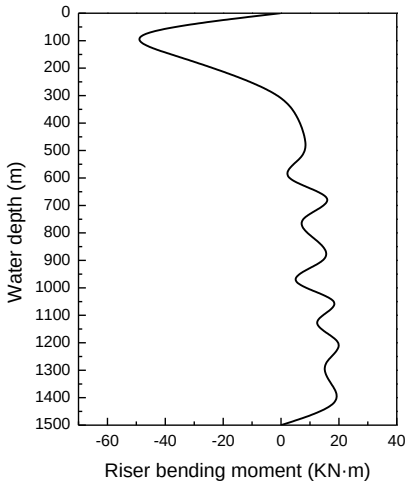
Water depth (m)
0
100
200
300
400
500
600
700
800
900
1000
1100
1200
1300
1400
1500
-60
-40
-20
0
20
40
Riser bending moment (KN·m)

b)

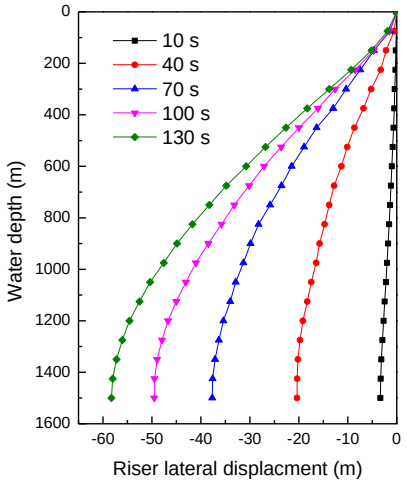
10 s
40 s
70 s
100 s
130 s
Water depth (m)
0
200
400
600
800
1000
1200
1400
1600
-60
-50
-40
-30
-20
-10
0
Riser lateral displacment (m)

c)

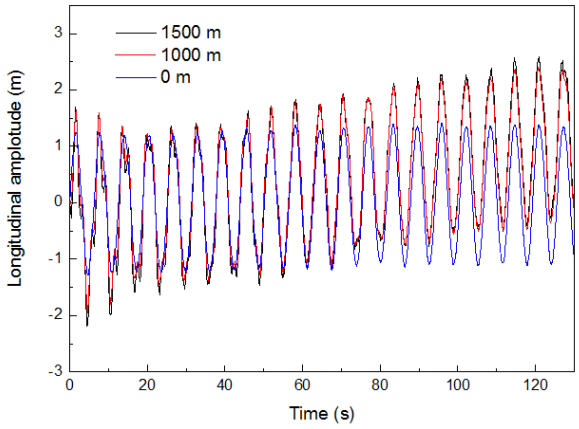

d)

Fig. 9 Hang-off riser mechanical behavior of the deepwater well in the South China Sea under the calculated ocean environment: a)–d) present the distributions of the riser lateral displacement, bending moment, dynamic lateral displacement from the upper flex joint to the seabed, and the longitudinal vibration at the bottom.

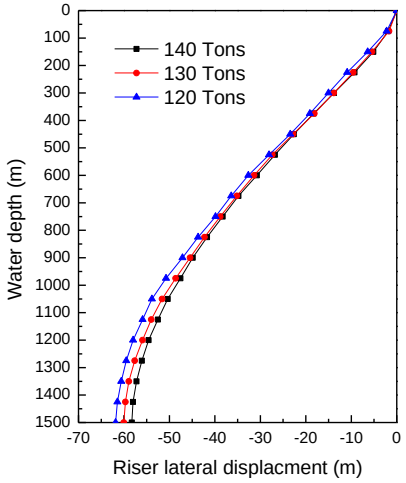

a)

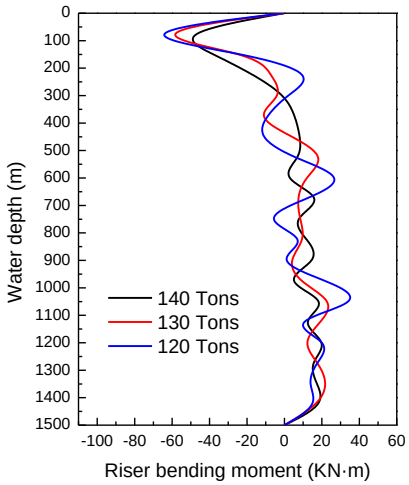

b)

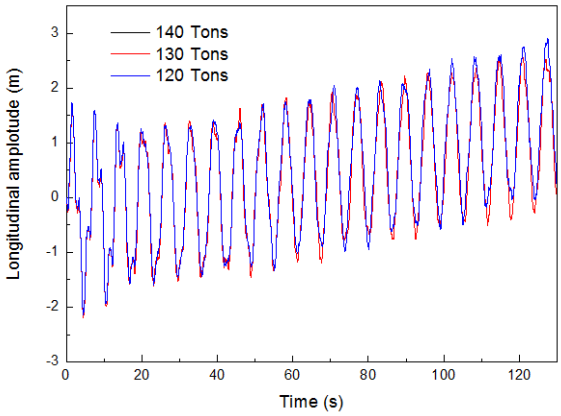

c)

Fig. 10 Hang-off riser mechanical behavior with the LMRP weight of 140, 130, and 120 Tons: a)–c) are the distributions of the riser lateral displacement, bending moment from the upper flex joint to the seabed, and the longitudinal vibration at the bottom.

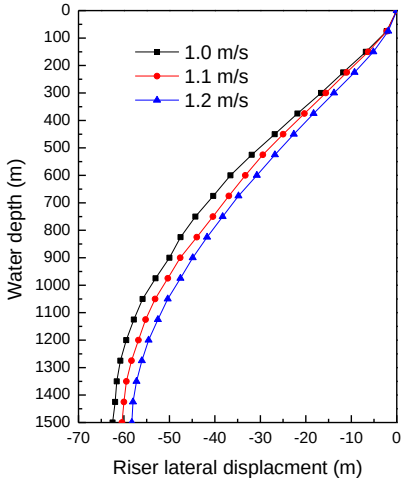

a)

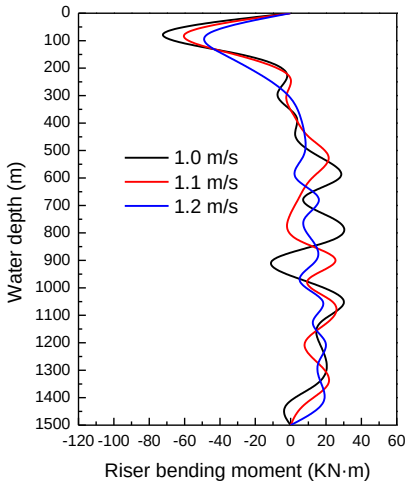

b)

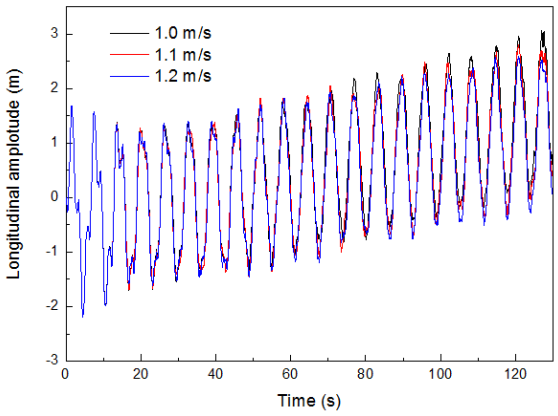

c)

Fig. 11 Hang-off riser mechanical behavior with the surface current speed of 1.0, 1.1, and 1.2 m/s: a)–c) are the distributions of the riser lateral displacement, bending moment from the upper flex joint to the seabed, and the longitudinal vibration at the bottom.

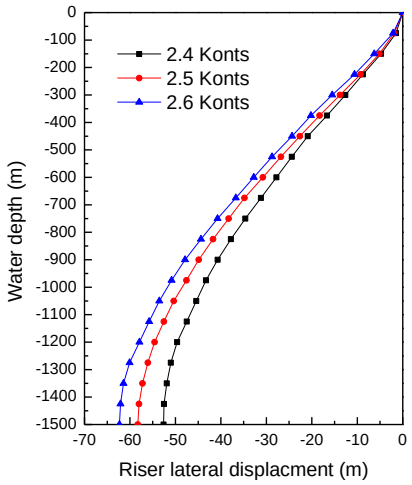

a)

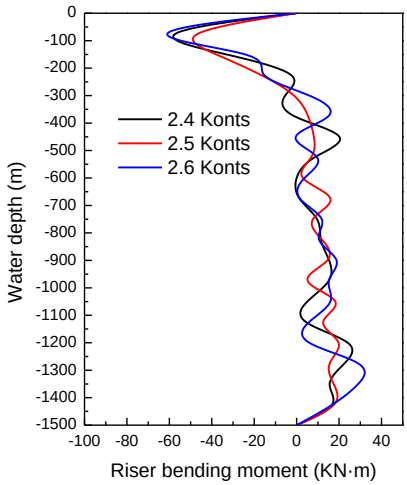

b)

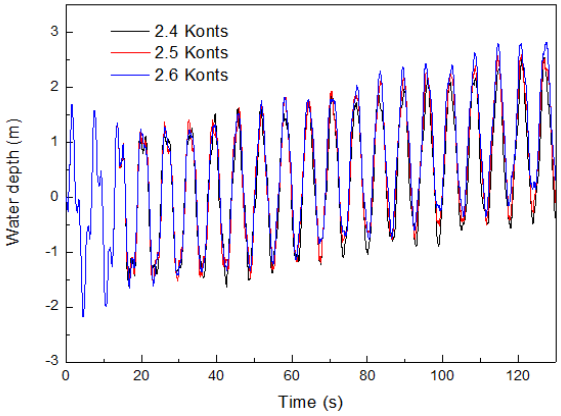

c)

Fig. 12 Hang-off riser mechanical behavior with the platform speed of 2.4, 2.5,and 2.6 Knots: a)–c) are the distributions of the riser lateral displacement, bending moment from the upper flex joint to the seabed, and the longitudinal vibration at the bottom.

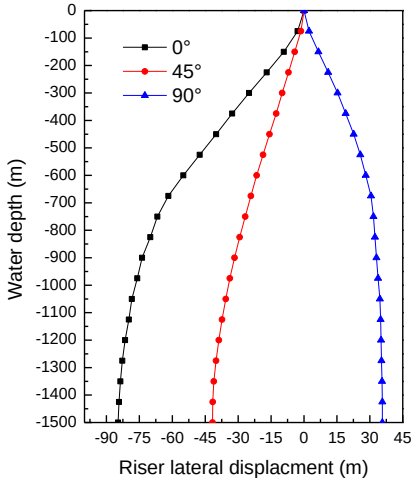

a)

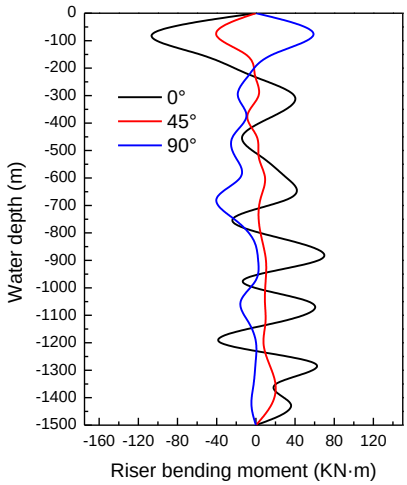

b)

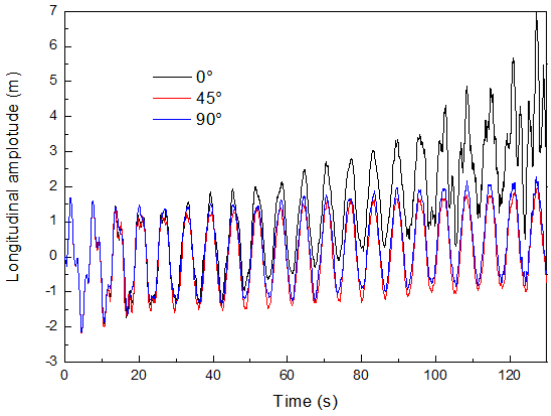

c)

Fig. 13 Hang-off riser mechanical behavior with the desired track of 0°, 45°, and 90°: a)–c) are the distributions of the riser lateral displacement, bending moment from the upper flex joint to the seabed, and the longitudinal vibration at the bottom.

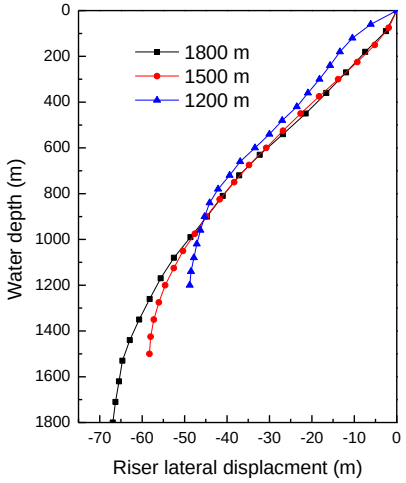

a)

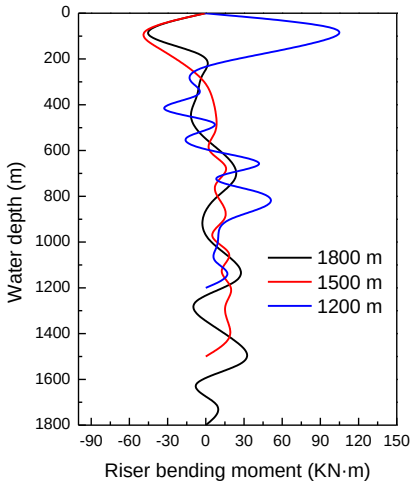

b)

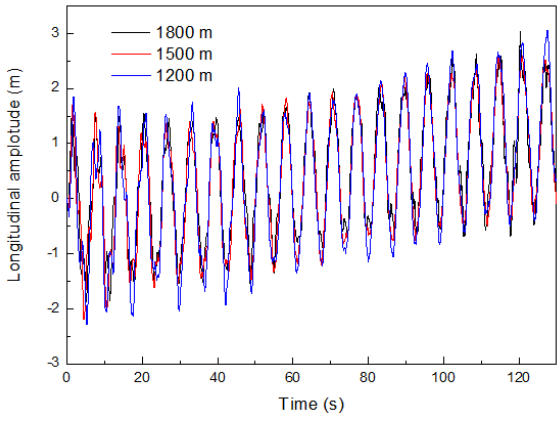

c)

Fig. 14 Hang-off riser mechanical behavior with the suspension length of 1200, 1500, and 1800 m: a)–c) are the distributions of the riser lateral displacement, bending moment from the upper flex joint to the seabed, and the longitudinal vibration at the bottom.